IOP Publishing Superconductor Science and Technology
Supercond. Sci. Technol. 31 (2018) 055007 (10pp) https://doi.org/10.1088/1361-6668/aab3be

Thermal coupling effect on the vortex dynamics of superconducting thin films: time-dependent Ginzburg–Landau simulations

Ze Jing[1], Huadong Yong[2] and Youhe Zhou[1,2]

[1] Research Center of Applied Mechanics, School of Mechano-Electronic Engineering, Xidian University, Xian, Shaanxi 710071, People's Republic of China
[2] Key Laboratory of Mechanics on Disaster and Environment in Western China, Ministry of Education of China, and Department of Mechanics and Engineering Sciences, College of Civil Engineering and Mechanics, Lanzhou University, Lanzhou, Gansu 730000, People's Republic of China

E-mail: zejing@xidian.edu.cn

Received 11 November 2017, revised 21 February 2018
Accepted for publication 2 March 2018
Published 29 March 2018

Abstract

In this paper, vortex dynamics of superconducting thin films are numerically investigated by the generalized time-dependent Ginzburg–Landau (TDGL) theory. Interactions between vortex motion and the motion induced energy dissipation is considered by solving the coupled TDGL equation and the heat diffusion equation. It is found that thermal coupling has significant effects on the vortex dynamics of superconducting thin films. Branching in the vortex penetration path originates from the coupling between vortex motion and the motion induced energy dissipation. In addition, the environment temperature, the magnetic field ramp rate and the geometry of the superconducting film also greatly influence the vortex dynamic behaviors. Our results provide new insights into the dynamics of superconducting vortices, and give a mesoscopic understanding on the channeling and branching of vortex penetration paths during flux avalanches.

Keywords: superconductor, vortex dynamics, TDGL equation, numerical simulations

(Some figures may appear in colour only in the online journal)

1. Introduction

Superconductors have been widely used in many application areas such as high magnetic field magnets [1], electric power devices [2] and superconducting electronics etc [3]. Most of the applicable superconducting materials belong to type-II. Under the external magnetic field, magnetic flux penetrates into the superconductor in the form of quantum flux lines (or vortices) [4]. Vortex dynamics are responsible for the entire electromagnetic properties of superconductors. Understanding the dynamics of vortices is crucial for the application of superconductors [5].

For type-II superconductors, the current density that can flow without dissipation is limited by the critical current density, which is determined by the pinning from material imperfections, interactions with other vortices and the Lorentz forces [4, 5]. According to the Bean's critical state model [6], vortices are statically pinned within the superconductor when the current density is below the critical current density. However, this critical state is metastable. Any tiny disturbance like thermal fluctuation will lead to the motion of vortices. The moving vortices dissipate energy and disturb the critical state [7–9]. If the dissipated energy cannot be timely removed, the local temperature of the superconductor increases, which weakens pinning and facilitates the motion of vortices even further. Thus, a positive feedback loop is formed where small disturbances develop into macroscopic thermomagnetic instabilities in the vortex matter [10]. Thermomagnetic

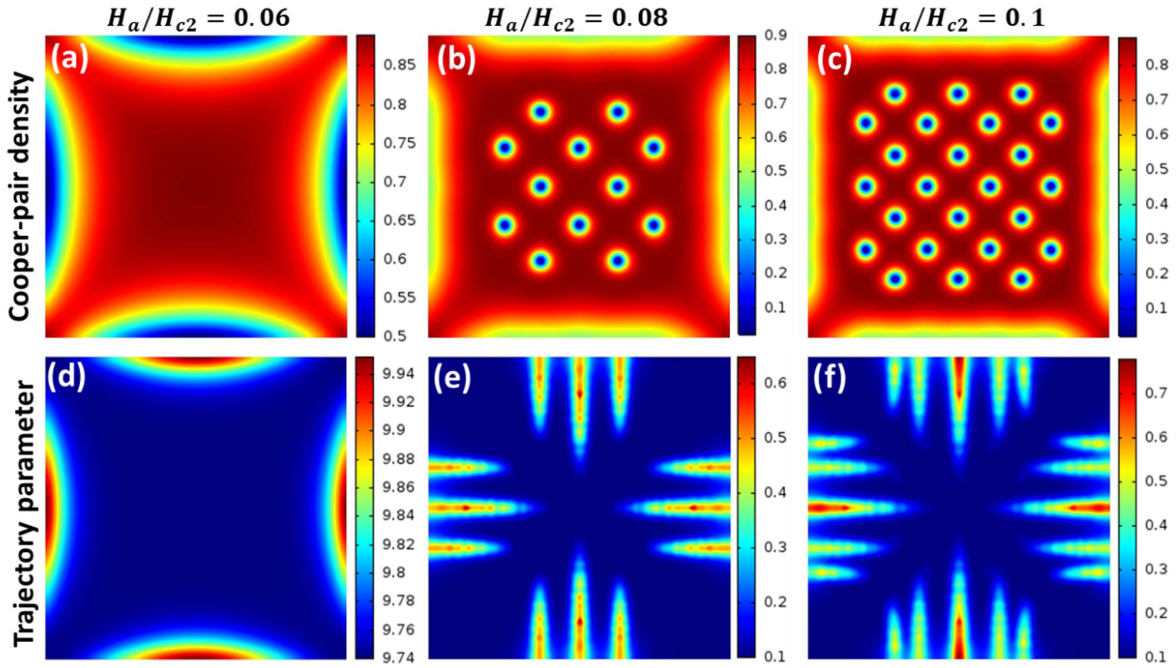

Figure 1. Distribution of the Cooper-pair density (a)–(c) and trajectory parameter (d)–(f) within a 60 × 60 superconducting thin film under the environment temperature $T_0 = 0.1\ T_c$. The film is subjected to an external magnetic field increased from zero to $H_a/H_{c2} = 0.1$ with the ramp rate $\dot{H}_a/H_{c2} = 1.0 \times 10^{-4}$. Here, the temperature is assumed constant throughout the film.

instability is a frequently encountered challenge during the application of superconducting devices [11–14]. Magneto-optical imaging (MOI) of many superconducting materials [15–21] has shown that the flux penetration paths during an avalanche event form branching structures. The flux front propatation speed can reach up to hundreds of $\mathrm{km\,s^{-1}}$ at the early stage of flux avalanches [17, 22]. The maximum temperature at the propagation front rises up to 1.2–1.4 times of the critical temperature T_c [22].

Research on the flux avalanches is important both for the fundamental understanding of vortex dynamics and for the application of superconducting devices. Linear stability analysis has been adopted to analyze the threshold conditions for the onset of thermomagnetic instability [23, 24]. Based on the coupled nonlinear equations for the non-local electrodynamics and the heat diffusion, the spatio-temporal evolution of the flux avalanches from its initial nucleation stage to the branching stage and finally the stagnation of flux motion are reproduced through numerical simulations [25–29]. From a mesoscopic point of view, thermomagnetic instability originates from the coupling between the fast-moving vortices and the motion induced energy dissipation. The detailed dynamics of individual vortices is essential to explore the physical mechanism of thermomagnetic instabilities. Many experiment methods, including STM [30, 31], magnetic force microscopy [32], MOI [33], scanning superconducting quantum interference device (SQUID) [34], scanning Hall probes [35, 36] and SQUID-on-tip [37], have been applied to image the vortex matter. Phenomena related to vortex dynamics like melting [38], plastic creep of the vortex lattice [30] and energy dissipation of single vortices [35] are found through experiments. Theoretically, the time-dependent Ginzburg–Landau (TDGL) theory has been widely used to explore the dynamics of superconducting vortices [39–43]. The relaxation dynamics of a quenched normal spot in a type-II superconductor are investigated based on the TDGL theory analytically and numerically [44]. Numerical solutions of the coupled TDGL equations and the heat diffusion equation show that heat dissipation leads to an increase of the hysteresis in the current–voltage characteristic of a mesoscopic superconducting sample with leads [45]. Non-equilibrium dynamics of superconducting detectors at the transition edge are examined by solving the TDGL equations coupled with heat-diffusion and Maxwell equations [46, 47]. Responses of superconducting thin films subjected to the abrupt switching on current are obtained by solving the TDGL equations. Different resistive modes, such as the flux-flow state (slow-moving vortices), phase-slip line state (fast-moving vortices) and hot-spot state are found depending on the applied current and temperature [48]. In addition, dynamic behaviors of vortices in the superconductors under oscillating magnetic field are also investigated using TDGL simulations [49]. Recently, the superfast dynamics and flow instabilities of magnetic vortices are imaged and studied by the numerical simulations of TDGL equations [50]. It is found that the fast-moving vortices form mesoscopic vortex channels which bifurcate as the current and magnetic field increases. The annihilation dynamics and heat diffusion of Abrikosov's vortex–antivortex pairs in a mesoscopic superconductor with a central hole are simulated by coupling the heat diffusion equation and the dissipated energy to the generalized TDGL equations [51]. While the dynamic behaviors of superconducting vortices have been extensively investigated by the TDGL theory, the physics of vortex dynamics during the flux

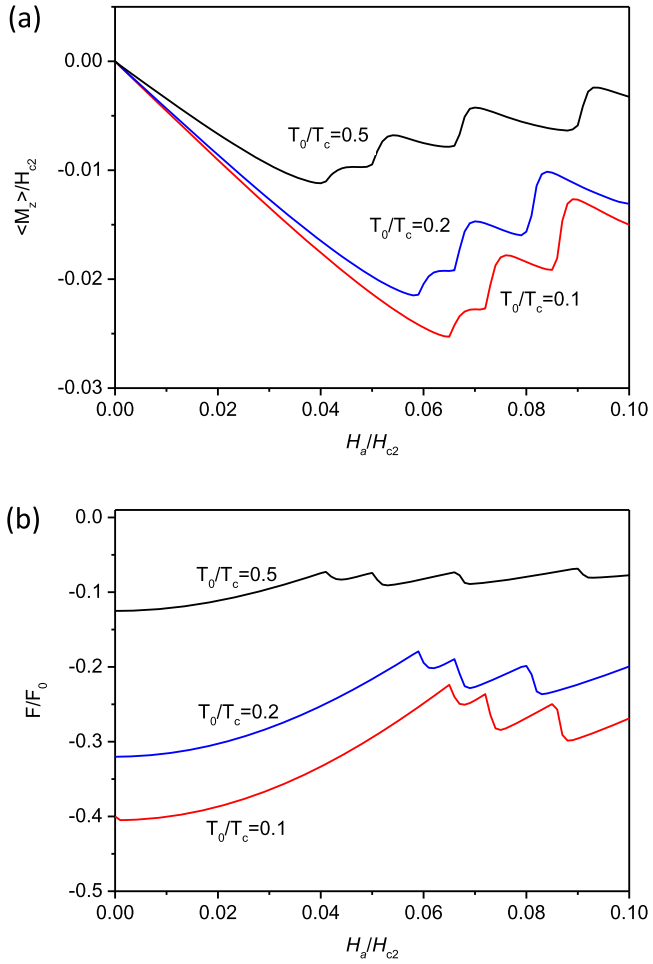

Figure 2. Average magnetization (a) and free energy (b) curves of the 60×60 superconducting thin film, at the environment temperature $T_0/T_c = 0.1, 0.2, 0.5$, respectively. The film is subjected the external magnetic ramped from zero to $H_a/H_{c2} = 0.1$ at the ramp rate $\dot{H}_a/H_{c2} = 1.0 \times 10^{-4}$. The temperature is assumed constant throughout the film.

avalanches remains largely unexplored. By performing TDGL simulations, the deflection in flux trajectories during the avalanche process of a thickness modulated superconducting thin film is demonstrated at the individual vortex level [21]. However, the vortex motion induced energy dissipation and the heat diffusion are neglected in the simulation. It is to be noted that both the fast motion of vortices and the motion induced energy dissipation play significant roles in the flux avalanches. Thus, the energy dissipation and heat diffusion have to be considered and coupled with the TDGL equations to understand the physical mechanism of thermomagnetic instabilities.

In this work, we investigate the ultrafast vortex dynamics of mesoscopic superconducting thin films subjected to an external magnetic field. The generalized TDGL equation is adopted to simulate the spatio-temporal evolution of vortices. We focus on the coupling between vortex motion and the motion induced energy dissipation. Factors that influence the vortex dynamics, such as the environment temperature, the magnetic field ramp rate, and geometry of the sample are discussed in detail. This paper is organized as follows. The theoretical formalisms used in the simulation is briefly introduced in section 2. Then, we show our numerical results and make detailed discussions on the vortex dynamics in section 3. Conclusions and summarizations of this work are presented in section 4.

2. Theoretical formalisms

The main ingredients of the flux avalanches are the vortex motion induced energy dissipation, the local heat diffusion, and the heat transfer through the coolant bath or the substrate. To interpret the flux avalanche behaviors at the individual vortex level, energy dissipation due to the induced electrical field and the relaxation of ψ should be considered. Therefore, we couple the generalized TDGL equations with the thermal diffusion equation to investigate the thermal effect on the vortex dynamics of superconductor thin films. Here, we present the basic equations adopted in the simulation.

2.1. TDGL equations for vortex dynamics

The dimensionless generalized TDGL equations with respect to the complex order parameter ψ and the vector potential $\boldsymbol{A}$ take the following form [52, 53]:

$$\frac{u}{\sqrt{1+\gamma^2|\psi|^2}}\left(\frac{\partial}{\partial t}+\frac{\gamma^2}{2}\frac{\partial|\psi|^2}{\partial t}+\mathrm{i}\varphi\right)\psi=(\boldsymbol{\nabla}-\mathrm{i}\boldsymbol{A})^2\psi+(1-T-|\psi|^2)\psi, \tag{1}$$

$$\kappa^2\nabla\times(\nabla\times\boldsymbol{A}-\mu_0\boldsymbol{H})=\boldsymbol{J}_s-\left(\frac{\partial\boldsymbol{A}}{\partial t}+\nabla\varphi\right), \quad \text{in } \Omega, \tag{2}$$

where $\overline{\psi}$ is the conjugate of order parameter ψ, T is the local temperature. The superconducting current density is defined as $\boldsymbol{J}_s=\frac{1}{2\mathrm{i}}(\overline{\psi}\boldsymbol{\nabla}\psi-\psi\boldsymbol{\nabla}\overline{\psi})-\boldsymbol{A}|\psi|^2$. In the above equations, the lengths are normalized by the coherence length ξ at zero temperature, the time is normalized by the Ginzburg–Landau relaxation time $t_0=\pi\hbar/8k_bT_cu$. The order parameter is normalized by $\psi_0=\alpha_0T_c/\beta$, where α_0 and β are the phenomenological Ginzburg–Landau parameters. The magnetic field is normalized by the upper critical magnetic field H_{c2} at zero temperature. The vector potential $\boldsymbol{A}$ is normalized by $H_{c2}\xi$. The scalar electric potential φ is normalized by $\hbar/2et_0$. The Ginzburg–Landau parameter $\kappa=\lambda/\xi$, where λ is the London penetration depth. The parameter u is related to the relaxation of ψ. Parameter $\gamma=2\tau_E\psi_0/\hbar$ takes into account the influence of inelastic phonon–electron scattering time τ_E on the superconducting vortex dynamics [52, 53].

The numerical simulations are implemented by using the following boundary conditions

$$(\boldsymbol{\nabla}-\mathrm{i}\boldsymbol{A})\psi\cdot\boldsymbol{n}=0, \quad \text{on } \partial\Omega, \tag{3}$$

$$\nabla\times\boldsymbol{A}\times\boldsymbol{n}=\mu_0\boldsymbol{H}_a\times\boldsymbol{n}, \quad \text{on } \partial\Omega, \tag{4}$$

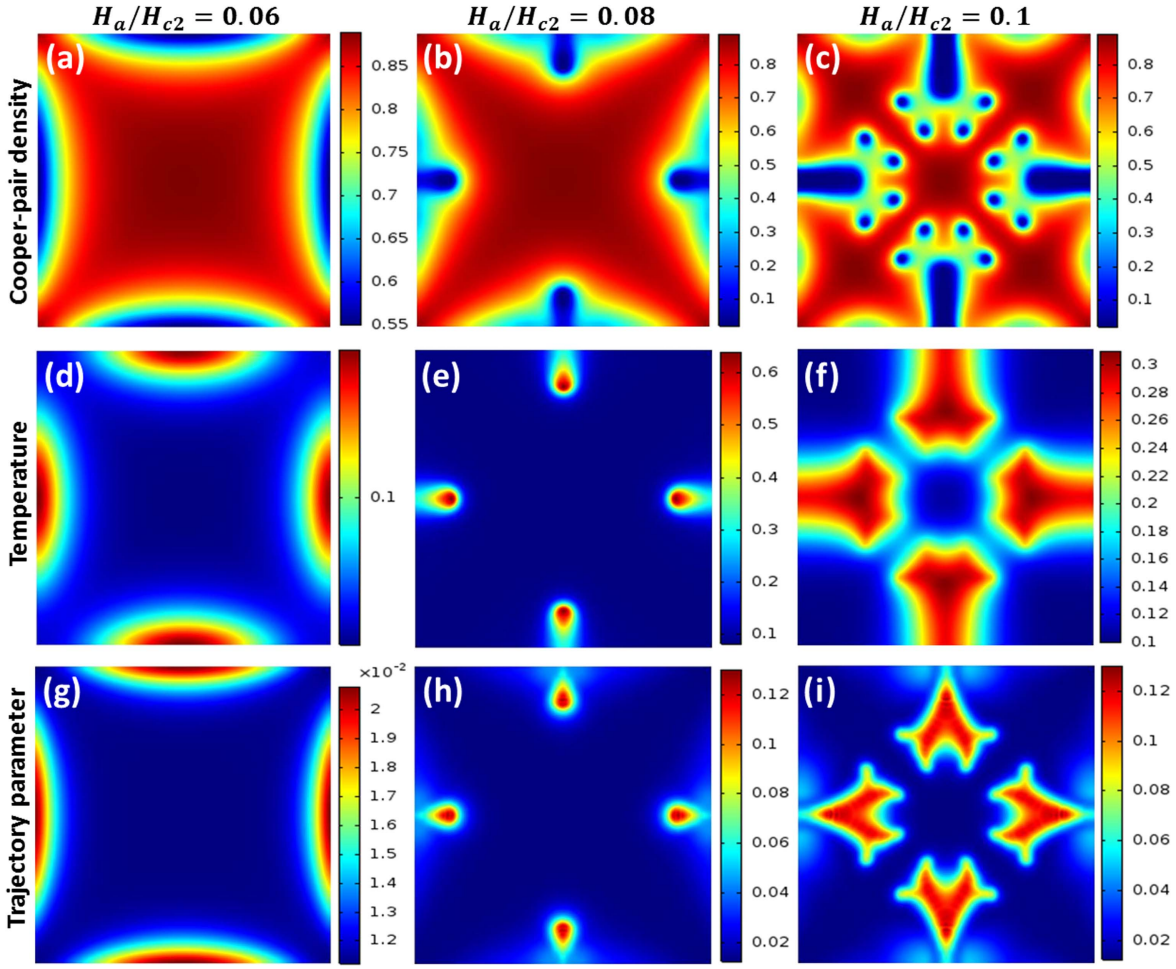

Figure 3. Distribution of Cooper-pair density (a)–(c), temperature (d)–(f) and trajectory parameter (g)–(i) within the 60 × 60 superconducting thin film at $T_0 = 0.1\ T_c$. The film is subjected to the external magnetic ramped from zero to $H_a/H_{c2} = 0.1$ with rate $\dot{H}_a/H_{c2} = 1.0 \times 10^{-4}$.

where $\boldsymbol{H}_a$ is the external magnetic field, $\boldsymbol{n}$ is the unit vector perpendicular to the boundary $\partial\Omega$.

The total free energy of the superconducting state is normalized by $F_0 = |\alpha|^2 V/\beta$, and can be derived as

$$F/F_0 = \int_\Omega \left[|\psi|^2 + \frac{1}{2}|\psi|^4 + |(-\mathrm{i}\nabla - \boldsymbol{A})\psi|^2 + \kappa^2 |\nabla \times \boldsymbol{A} - \mu_0 \boldsymbol{H}|^2 \mathrm{d}\Omega \right]. \quad (5)$$

Trajectories of the superconducting vortices are captured by the parameter $S(x, y)$, which is defined as the root mean square of the rate of changes in the local Cooper-pair density: $S(x, y) = \sqrt{\frac{1}{t_2 - t_1}\int_{t_1}^{t_2} \left(\frac{\partial |\psi(x, y)|^2}{\partial t} \right)^2 \mathrm{d}t}$, where t is the time variable and $t_2 - t_1$ is the time integration interval [21, 54]. The parameter S at a given point (x, y) strongly increases when a moving vortex passing by.

2.2. Heat diffusion equation

The change of local temperature due to the dissipated energy is considered by coupling the following dimensionless heat diffusion equation to equations (1) and (2) [45]

$$C_{\mathrm{eff}} \frac{\partial T}{\partial t} = \nabla \cdot (\kappa_{\mathrm{eff}} \nabla T) + \frac{1}{2} W_{\mathrm{total}} - \eta (T - T_0), \quad (6)$$

where T_0 is the environment temperature, C_{eff} is the effective heat capacity, K_{eff} is the effective thermal conductivity, η is the heat transfer coefficient of the substrate, and W_{total} represents the heat source from vortex motion induced energy dissipation. For a superconductor subjected to an external magnetic field, W_{total} can be obtained by the Helmholtz free energy theorem and expressed in the following dimensionless form [55]

$$W_{\mathrm{total}} = 2\left(\frac{\partial \boldsymbol{A}}{\partial t}\right)^2 + \frac{2u}{\sqrt{1 + \gamma^2 |\psi|^2}} \left[\left(\left| \frac{\partial \psi}{\partial t} \right| \right)^2 + \frac{\gamma^2}{4} \left(\frac{\partial |\psi|^2}{\partial t} \right)^2 \right] \quad (7)$$

in which the first term represents the energy dissipation due to the induced electric field, and the second term is related to the relaxation of the order parameter. Here, the dissipated energy is normalized by $W_0 = H_{c2}^2(0)/[8\pi\kappa^2 t_0]$.

3. Numerical results and discussions

In the modeling, we consider the superconducting thin film with thickness d of 1–5 nm, which is much smaller than the coherence length ξ ($\sim$40 nm for the Nb sample) and penetration depth λ. In this case, the diamagnetization effect for the applied magnetic field and the thickness dependence of the order parameter and vector potential can be neglected in the simulation. Thus, the variation of the order parameter ψ, vector potential $\boldsymbol{A}$, and the temperature T with the film thickness is neglected. A two-dimensional model is adopted in the simulation. To reveal the thermal effects on the vortex dynamics and branching of the vortex trajectories during flux avalanches, we consider the following two cases. First, the temperature is assumed constant throughout the thin film. The coupling between vortex motion and energy dissipation is neglected in the simulation. Second, the energy dissipation induced by the vortex motion and the thermal coupling effects on the vortex dynamics are taken into account.

3.1. Vortex dynamics of perfect superconducting thin film

When the parameters $u = 1.0$ and $\gamma = 0$, the generalized TDGL equations degenerate into the ordinary TDGL equations in which the energy dissipation is not considered. Thus, the numerical simulations of vortex dynamics at constant temperature are carried out by adopting $u = 1.0$, $\gamma = 0$ and $\kappa = 10.0$. Here, we present the simulation results performed on a superconducting thin film of sizes 60×60. In figure 1, we show the distribution of superconducting vortices and the vortex trajectories of the film. The film is subjected to an external magnetic field which increases from zero to $H_a/H_{c2} = 0.1$ with the ramp rate $\dot{H}_a/H_{c2} = 10^{-4}$, under the environment temperature $T_0/T_c = 0.1$. For the quantities presented in the following images, the red color corresponds to the highest value, while the blue color corresponds to the lowest value. Figures 1(a)–(c) show the distribution of Cooper-pair density (which is proportional to the square modulus of the order parameter, $|\psi|^2$) as the external magnetic field ramped from zero to $H_a/H_{c2} = 0.06$, 0.08 and 0.1 respectively. The corresponding trajectories of the superconducting vortices captured by the parameter $S(x, y)$ are shown in figures 1(d)–(f). As shown in figures 1(a)–(c), the superconducting thin film is initially in a vortex free state at the zero external magnetic field. When the external magnetic field $H_a = 0.065H_{c2}$, vortices start to penetrate into the film. If the magnetic field continues to increase, the film is filled with four vortices initially. As the magnetic field increases even further, the film is filled with 8 vortices at the outer of the existing vortices (see figure 1(b)). Then, vortices will fill internal shells until the number of vortices gets large enough to create outer shells. These simulated vortex configurations are consistent with the scanning electron microscope images of the mesoscopic superconducting thin film reported in [56]. Furthermore, it is clearly seen from figures 1(d)–(f) that the vortices penetrate into the film from center region of the sample edges. The trajectories of vortices are straight and perpendicular to the film edges. Figures 2(a) and (b) show the

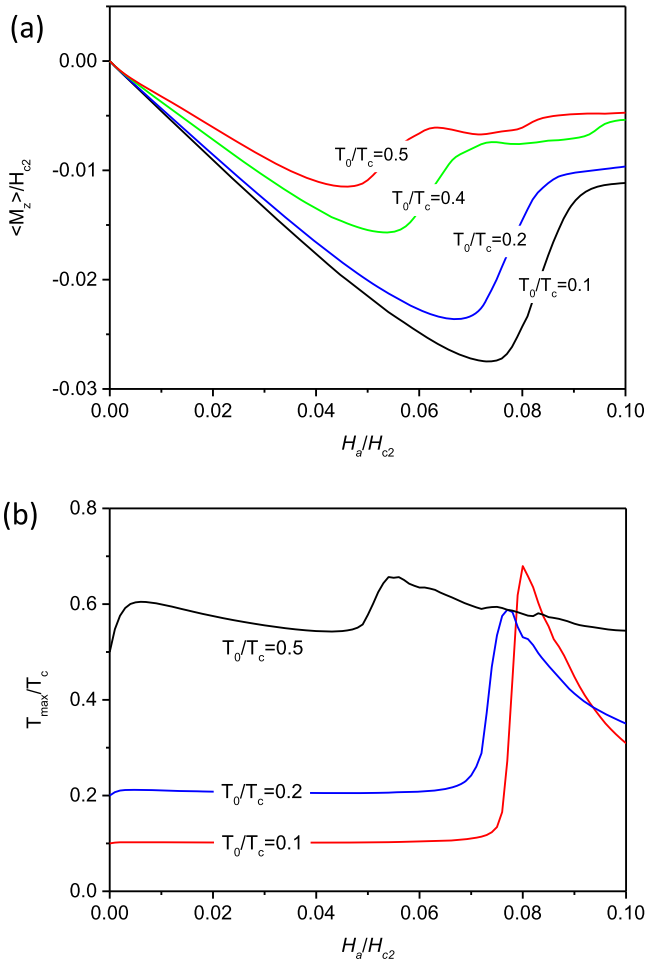

Figure 4. Average magnetization (a) and maximum temperature (b) curves of the 60×60 superconducting thin film at the environment temperature $T_0/T_c = 0.1$, 0.2, 0.5, respectively. The film is subjected to the external magnetic field ramped from zero to $H_a/H_{c2} = 0.1$ with the rate $\dot{H}_a/H_{c2} = 1.0 \times 10^{-4}$.

average magnetization $\langle M_z \rangle$ versus applied magnetic field $M(H)$ curves and the free energy versus applied magnetic field $F(H)$ curves for the system at different temperatures. As shown in figure 2(a), the $M(H)$ curves jump as the external magnetic field increases. Jumping in the average magnetization curve corresponds to the transition between states with different number of vortices. When the external magnetic field increases, more and more vortices enter into the superconductor. As the applied field increases, the vortices already existing within the superconductor film do not allow room for more vortices. This made the superconductor diamagnetic again even if the the applied magnetic field increases. In addition, it can be seen that the higher the environmental temperature, the earlier the magnetization jumps and the smaller the absolute value of the magnetization.

In order to consider the energy dissipation from vortex motion, we use the parameters $u = 5.79$, $\gamma = 10$ and $\kappa = 10.0$ to solve the generalized TDGL equations. Then, the heat diffusion equation (6), which is coupled with the generalized TDGL equations through energy dissipation expression (7), is solved by using the parameters $K_{\text{eff}} = 0.06$, $C_{\text{eff}} = 0.65$ and

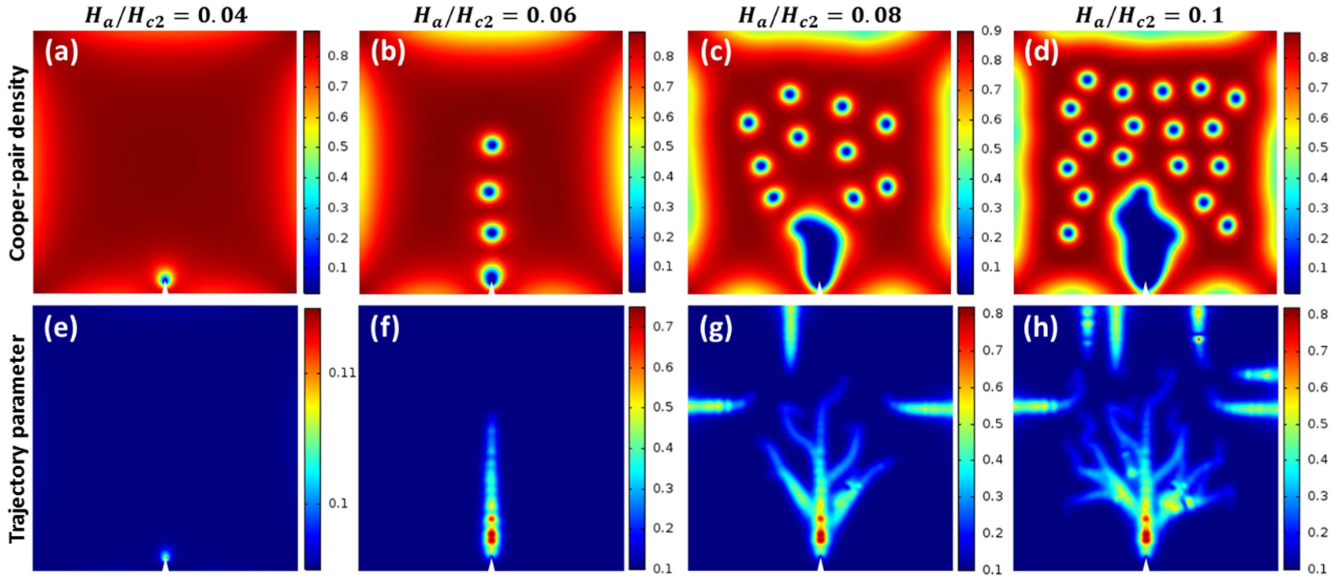

Figure 5. Distribution of the Cooper-pair density (a)–(d) and trajectory parameter (e)–(h) of a 60 × 60 superconducting thin film with a edge defect, at the environment temperature $T_0 = 0.1\ T_c$. The film is subjected to the external magnetic field ramped from zero to $H_a/H_{c2} = 0.1$ at the rate $\dot{H}_a/H_{c2} = 1.0 \times 10^{-4}$. The temperature is assumed constant throughout the film.

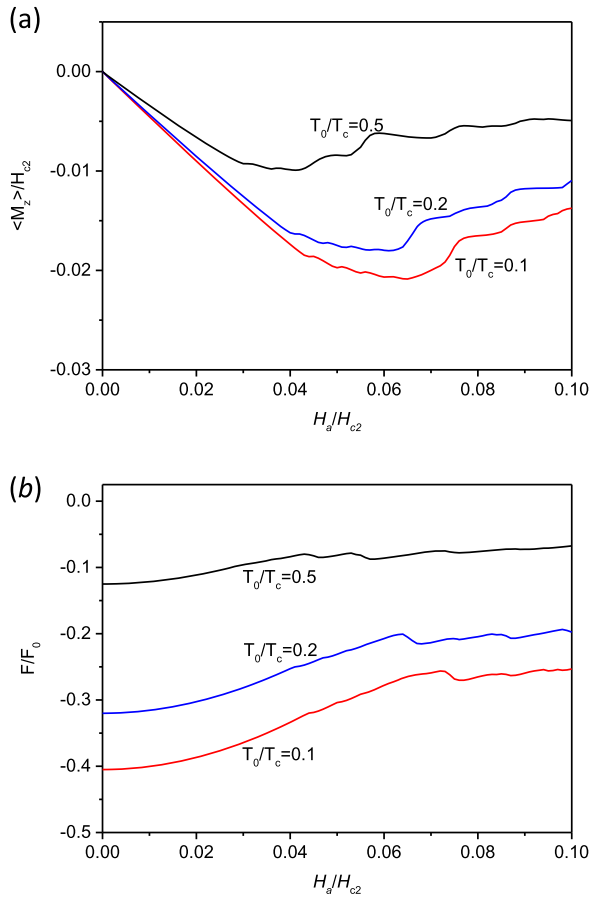

Figure 6. Average magnetization (a) and free energy (b) of the 60 × 60 superconducting thin film with an edge defect. The film is subjected to the external magnetic field ramped from zero to $H_a/H_{c2} = 0.1$ with the ramp rate $\dot{H}_a/H_{c2} = 1.0 \times 10^{-4}$ at the environment temperature $T_0/T_c = 0.1$, 0.2, 0.5 respectively. The temperature is assumed constant throughout the film.

$\eta = 2 \times 10^{-3}$. Figure 3 shows the distribution of Cooper-pair density $|\psi|^2$ (see figures 3(a)–(c)), the temperature T (see figures 3(d)–(f)), and the trajectory parameter S (see figures 3(g)–(i)) of the superconducting film during the magnetic field increasing process. Comparing the distribution of Cooper-pair density $|\psi|^2$ and the trajectory parameter $S(x, y)$ shown in figures 3 and 1, we can obviously see that thermal coupling has significant effects on the vortex dynamics of the superconducting thin film. As seen from figures 3(a)–(c), vortices penetrate into the film from the center of the sample edges. However, there is only one penetration site at each film edges when the thermal coupling effect is considered. And, the magnetic vortices obviously show a droplet shape in the early stage of the vortex penetration, which is quite different from the results obtained without consideration of the thermal effect. As the external magnetic field increases, more vortices rush in and the vortex penetration 'channels' form in the film. In addition, we can easily see from figures 3(c), (f) and (i) that the vortex penetration path branches when the external magnetic field increases over a critical value. These can be attributed to the following two mechanisms which have not been reported by experiments and coarse-grained numerical simulations. The fast-moving vortices leave behind reduced order parameters which attract the following vortices. Thus, vortex chains formed into channels of reduced Cooper-pair density. Another mechanism is that the motion of vortex dissipates energy, the energy dissipated by each vortex forms a channel of enhanced temperature along the vortex trajectory. The vortices penetrating from the film edges slow down as it moves along the channel. The subsequent penetrating vortices move along the same trajectory, causing jamming near the region where vortices slow down. Thus, the mutual repulsion between vortices either pushes them further along the channels or causes bifurcation of the channels into branches.

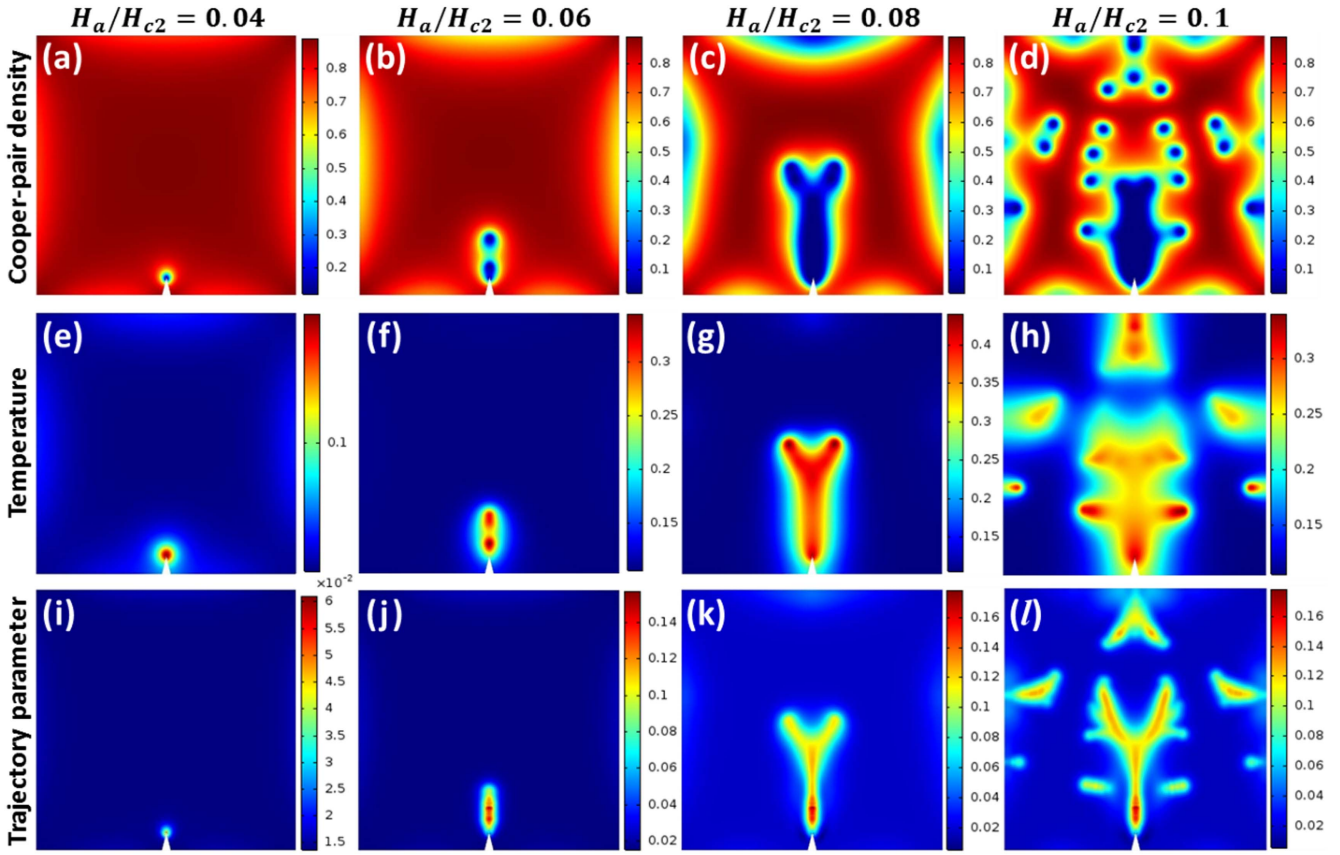

Figure 7. Distribution of the Cooper-pair density (a)–(d), temperature (e)–(h) and trajectory parameter (i)–(l) within the 60 × 60 superconducting thin film, which contains a triangular edge defect and subject to the external magnetic field ramped from zero to $H_a/H_{c2} = 0.1$ with the rate of $\dot{H}_a/H_{c2} = 1.0 \times 10^{-4}$ at $T_0 = 0.1\ T_c$.

In figure 4, we present the magnetization versus applied magnetic field, $M(H)$ (see figure 4(a)) and the maximum temperature versus applied magnetic field $T_{max}(H)$ (see figure 4(b)) curves of the thin film under different environment temperatures. Comparing the *M(H)* curves shown in figures 4(a) and 2(a), we can conclude that the magnetization curve gets smoother when the energy dissipation by the vortex motion is considered in the simulation. From figure 4(b), we can see that the maximum temperature sharply increases as the magnetic vortices start to penetrate into the sample. As time goes on, increasing magnitude of the temperature diminishes. And, the lower the environmental temperature the larger magnitude the temperature increases. This is consistent with the experimental results of flux avalanches. It is found that the lower the environmental temperature the larger the local temperature increases during a flux avalanche process.

3.2. Vortex dynamics of superconducting thin film with edge defect

It is known that the magnetic vortices always nucleate and propagate into the superconductors from weak points like edge defects etc. Here, we make numerical simulations on the vortex dynamics of the superconducting film with a triangular edge defect.

First, we neglect the vortex motion induced thermal effect by adopting the same parameters $u = 1.0$, $\gamma = 0$ and $\kappa = 10.0$ as in section 3.1. In figure 5, we present the Cooper-pair density and the trajectory parameter distribution in the film subjected to an increasing magnetic field with ramp rate $\dot{H}_a = 10^{-4}H_{c2}$. As expected, the magnetic vortices initially nucleate at the tip of the edge defect (see figures 5(a) and (e)). When the external magnetic field increases, more and more magnetic vortices nucleate at the tip of the defect, and propagate into the film following a straight line (see figures 5(b) and (f)). This can be explained by the fact that the moving vortices leaving behind a chain of reduced order parameter which attracts the subsequent vortices. Due to the preferred nucleation site of vortices, the vortex penetration channel is more obvious for the film with edge defect than that without edge defect. As shown in figures 5(c) and (g)), the magnetic flux vortex penetration path (i.e. the trajectory) bifurcates when the external magnetic field increases further. And, large amounts of vortices penetrate deep into the superconducting sample along the channels previously formed. Comparing the vortex configuration shown in figures 5(a)–(d) and 1(a)–(c), it is clearly seen that the edge defect has a significant effect on the vortex dynamics. The vortices rush in leads to the variation in average magnetization and total free energy of the superconductor. Figure 6 shows the average magnetization and the free energy curve of

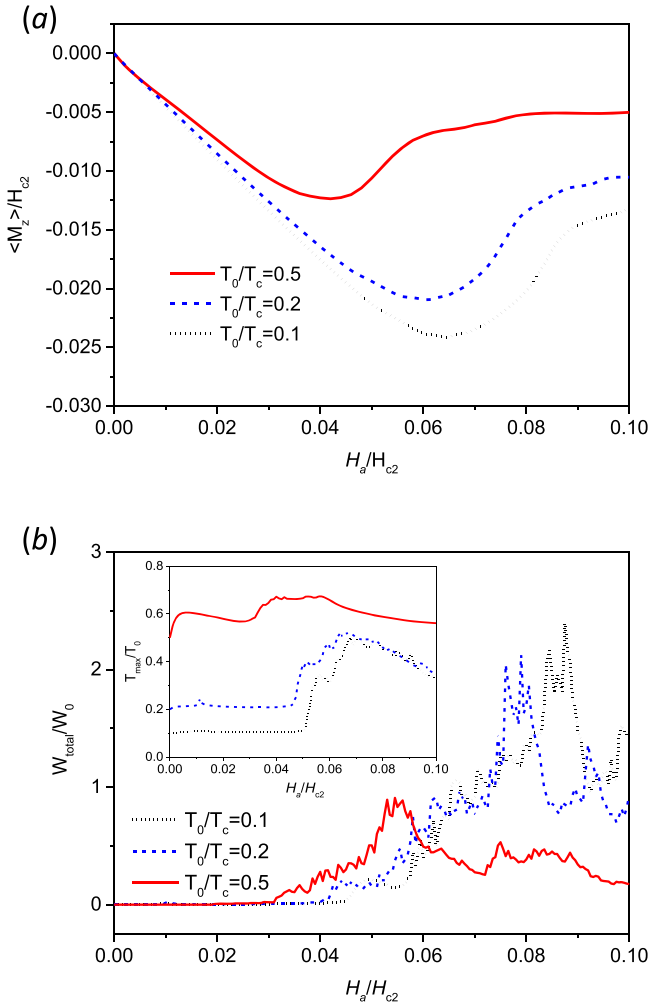

Figure 8. Average magnetization (a) and dissipation energy (b) curves of a 60 × 60 superconducting thin film with a triangular edge defect subjected to the external magnetic field ramped from zero to $H_a/H_{c2} = 0.1$ with the rate of $\dot{H}_a/H_{c2} = 1.0 \times 10^{-4}$, at $T_0/T_c = 0.1, 0.2, 0.5$. The insets shown in (b) is the maximum temperature curve.

the film at different environment temperatures. From figures 6(a) and (b), we can see that the average magnetization and free energy curves of the sample with edge defect have smaller wavy structures compared with these shown in figures 2(a) and (b) for the perfect film. Presence of the edge defect breaks geometrical symmetry of the superconducting square. As the external magnetic field increases, magnetic flux vortices first nucleate and then inject into the film through edge defect sequentially. Meanwhile, vortices penetrate into the perfect film from center of all the edges simultaneously. Thus, the overall jumping amplitude in the magnetization and free energy curve is smaller for the film with edge defect.

In addition, we have also investigated the thermal effect on the vortex dynamics of superconducting film with defect. The energy dissipation from the vortex motion is considered by adopting the parameters $u = 5.79$, $\gamma = 10$ and $\kappa = 10.0$ in the generalized TDGL equations. The thermal equation is coupled with the generalized TDGL solutions using the same parameters as for the perfect film. In figure 7, we present the Cooper-pair density, temperature and trajectory parameter distribution in the superconducting sample with edge defect. In contrast to the perfect film, the vortex penetration process of the film with edge defect is quite different. Moreover, the vortex motion induced energy dissipation play an important role in the vortex penetration. The magnetic vortices initially nucleate from the edge defect, and then penetrate further into the film along a straight line as the external magnetic field increases. Under certain external magnetic field ($H_a/H_{c2} = 0.07$) the vortex penetration path diverges at the flux propagation front (see figures 7(c), (g) and (k)). When the external field increases higher enough, vortices nucleate and propagates into the sample also from other boundaries without defect (figures 7(d), (h) and (l)). Figures 8(a) and (b) show the average magnetization and the dissipated energy of the superconducting film at different environment temperature. The inset of figure 8(b) shows maximum temperature versus applied magnetic field curve. Like that of the perfect film, the magnetization curve gets smoother when the thermal coupling effect is considered in the simulation. From the magnetization curve, it can be seen that the larger the environment temperature, the smaller the average magnetization of the thin film. Under a higher environment temperature, rising of the temperature gets smaller and the jump frequency of the temperature gets lower. From the energy dissipation curve, we can also see that the higher the environment temperature the lesser the overall energy dissipated due to the vortex motion.

3.3. Influence factors of vortex dynamics

As reported, the environment temperature, the external magnetic field ramp rate [57], and the geometry of the sample [58, 59] have significant effects on the vortex matter and flux avalanche behavior of superconductors. In this section, the influences of magnetic field ramp rate and the geometry size on the vortex dynamics of the film are considered.

The magnetic field ramp rate has great influences on the vortex dynamics of the superconducting film. In figure 9, we present the maximum temperature, the average magnetization (see the insets of figure 9(a)), and the trajectory parameters (figures 9(b)–(d)) of a 120 × 120 superconducting thin film under the environment temperature $T_0/T_c = 0.1$. It is found that the larger the magnetic field ramp rate, the higher the local temperature rises. In addition, variation in the temperature curve gets sharper at a lower magnetic field ramp rate. From the trajectory parameters distribution in figures 9(b)–(d), we can found that the main branch in the vortex trajectory gets more fractal under a lower magnetic field ramp rate. When the magnetic field ramp rate is low enough ($\dot{H}_a/H_{c2} = 0.2 \times 10^{-4}$), the branch patterns of the trajectory parameter is close to that shown in figure 5(h).

Figure 10 shows the maximum temperature $T_{max}(H)$ and the average magnetization $M(H)$ curve of the superconducting film (of geometry size 120 × 120) with an edge defect and under the environment temperature $T_0/T_c = 0.1$. It is seen that the overall tendency of the $T_{max}(H)$ and $M(H)$ curves are similar to that of the film of geometric size 60 × 60. Comparing the magnetization of the film with a smaller size, the average

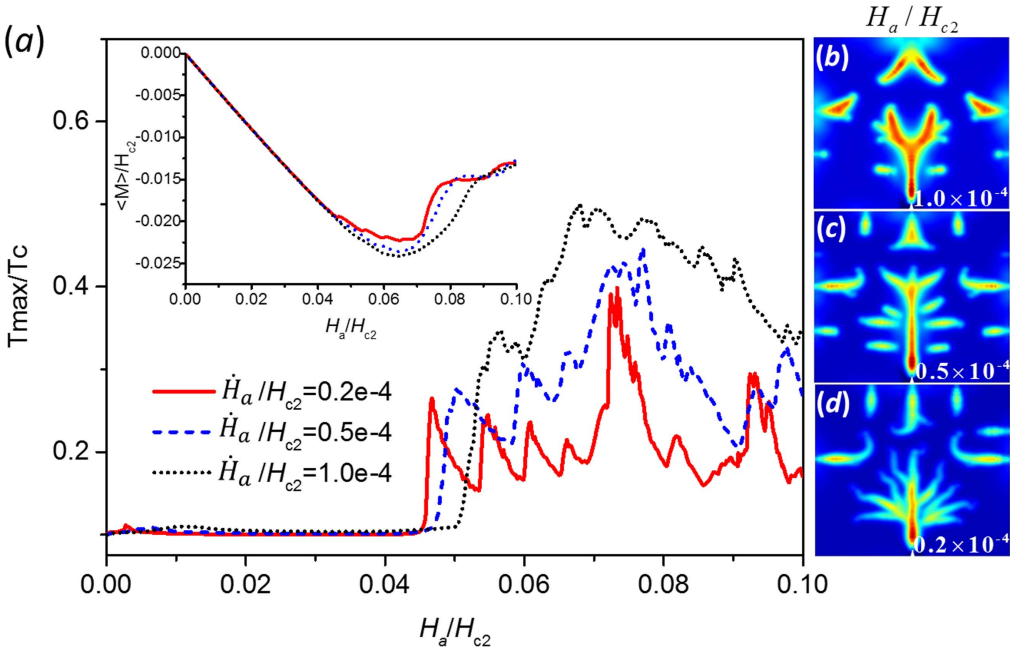

Figure 9. Maximum temperature curve (a) and the distribution of trajectory parameters (b)–(d) of the 120 × 120 superconducting thin film at $H_a/H_{c2} = 0.1$, under the environment temperature $T_0 = 0.1T_c$. Insets of (a) show the average magnetization curve. Here, the external magnetic filed is ramped from zero to $H_a/H_{c2} = 0.1$ at the rate $\dot{H}_a/H_{c2} = 0.2 \times 10^{-4},\ 0.5 \times 10^{-4},\ 1.0 \times 10^{-4}$ respectively.

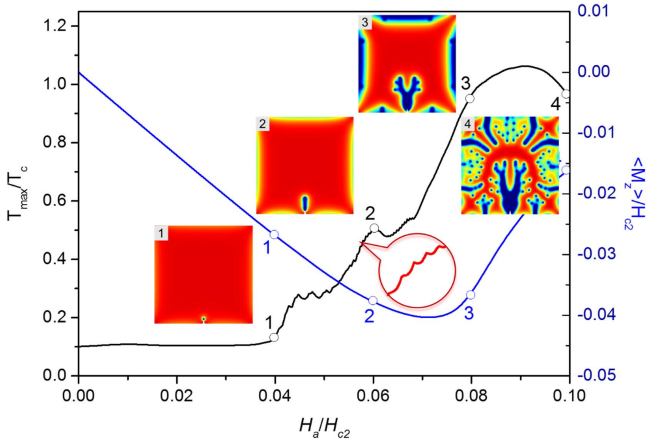

Figure 10. Maximum temperature and average magnetization curves of a 120 × 120 superconducting thin film with edge defect. The insets (1)–(4) show the Cooper-pair density distribution at $H_a/H_{c2} = 0.04, 0.06, 0.08, 0.1$ respectively. The film is subjected to an external magnetic field ramped from zero to $H_a/H_{c2} = 0.1$ with the rate $\dot{H}_a/H_{c2} = 1.0 \times 10^{-4}$ at the environment temperature $T_0 = 0.1\ T_c$.

magnetization of the 120 × 120 film is smaller. In addition, the larger film shows higher maximum temperature during the vortex penetration process. This is due to the fact that for the larger film the boundary effect gets weaker and the vortices become easier to enter into the film. The insets 1, 2, 3 and 4 show the corresponding vortex distributions in the film when the external magnetic field increases from zero to $H_a/H_{c2} = 0.04$, 0.06, 0.08 and 0.1 respectively. It is obviously seen that the flux avalanches also occur to a mesoscopic system with a larger size. From these vortices evolution pictures, we can see more branched vortex penetration paths of the film with a larger size than the smaller one. And, the superconducting thin film with a larger size shows more pronounced flux avalanche patterns.

4. Conclusions

In conclusion, the generalized time dependent Ginzburg–Landau equations are coupled with the heat diffusion equation to analyze the vortex dynamics of a mesoscopic superconducting thin film system. The vortex motion induced energy dissipation is considered in the simulation. The thermal coupling effect on the vortex dynamics of the perfect superconducting thin film and the film with edge defect are investigated. The simulation results show that thermal coupling has significant effects on the vortex motion of superconducting films. The physical mechanism for the bifurcation of vortex trajectories during the flux avalanches is explained at the individual vortex level, which has not been reported by the experiments and coarse-grained numerical simulations. On one hand, the fast-moving vortices leave behind a chain of reduced order parameter, which attracts the following vortices to form penetration channels. On the other hand, the fast-moving vortices dissipate energy and leave behind a channel of enhanced temperature. The velocity of other vortices moving along the channel slows down, which results in the jamming of vortices. And, the mutual repulsion of the jamming vortices causes the bifurcation of the vortex penetration channels. In addition, we have made detailed discussions on the factors that influencing the vortex dynamic behaviors. Influences of the environment temperature, the magnetic field ramp rate, and the geometry of the film on the vortex dynamics are discussed in detail. The simulation results show that the edge

defects always act as vortex nucleation site and through which magnetic vortices initially penetrates into the film. As the external magnetic field ramp rate gets higher, more energy dissipated due to the vortex motion. Our results add new insights into the thermomagnetic instability of superconductors from the individual vortex level.

Acknowledgments

We acknowledge the support from the National Natural Science Foundation of China (Nos. 11472120, 11572232, and 11602185) and the Fundamental Research Funds for the Central Universities (No. JB160404, JBG160401, XJS16043).

ORCID iDs

Ze Jing https://orcid.org/0000-0002-2030-4445
Huadong Yong https://orcid.org/0000-0002-0304-3191

References

[1] Senatore C, Alessandrini M, Lucarelli A, Tediosi R, Uglietti D and Iwasa Y 2014 *Supercond. Sci. Technol.* **27** 26
[2] Larbalestier D, Gurevich A, Feldmann D M and Polyanskii A 2001 *Nature* **414** 368–77
[3] Tolpygo S K 2016 *Low Temp. Phys.* **42** 361–79
[4] Tinkham M 2004 *Introduction to Superconductivity* 2nd edn (New York: McGraw-Hill)
[5] Moshchalkov V V, Woerdenweber R and Lang W 2010 *Nanoscience and Engineering in Superconductivity* (Berlin: Springer)
[6] Bean C P 1964 *Rev. Mod. Phys.* **36** 31–9
[7] Mints R G and Rakhmanov A L 1981 *Rev. Mod. Phys.* **53** 551–92
[8] Anderson P W and Kim Y B 1964 *Rev. Mod. Phys.* **36** 39–43
[9] Pannetier-Lecoeur M and Fermon C 2005 *Phys. Rev.* B **72** 180501
[10] Altshuler E and Johansen T H 2004 *Rev. Mod. Phys.* **76** 471–87
[11] Zhao Z W *et al* 2002 *Phys. Rev.* B **65** 064512
[12] Mohler G and Stroud D 1999 *Phys. Rev.* B **60** 9738–43
[13] Baziljevich M, Baruch-El E, Johansen T H and Yeshurun Y 2014 *Appl. Phys. Lett.* **105** 0003–6951
[14] Song H H, Hunte F and Schwartz J 2012 *Acta Mater.* **60** 6991–7000
[15] Jooss C, Albrecht J, Kuhn H, Leonhardt S and Kronmuller H 2002 *Rep. Prog. Phys.* **65** 651–788
[16] Johansen T H *et al* 2002 *Europhys. Lett.* **59** 599–605
[17] Bolz U, Biehler B, Schmidt D, Runge B U and Leiderer P 2003 *Europhys. Lett.* **64** 517–23
[18] Rudnev I A, Antonenko S V, Shantsev D V, Johansen T H and Primenko A E 2003 *Cryogenics* **43** 663–6
[19] Wimbush S C, Holzapfel B and Jooss C 2004 *J. Appl. Phys.* **96** 3589–91
[20] Rudnev I A, Shantsev D V, Johansen T H and Primenko A E 2005 *Appl. Phys. Lett.* **87** 042502
[21] Brisbois J *et al* 2017 *Phys. Rev.* B **95** 094506
[22] Vestgården J I, Shantsev D V, Galperin Y M and Johansen T H 2012 *Sci. Rep.* **2** 886
[23] Denisov D V, Rakhmanov A L, Shantsev D V, Galperin Y M and Johansen T H 2006 *Phys. Rev.* B **73** 014512
[24] Denisov D V *et al* 2006 *Phys. Rev. Lett.* **97** 077002
[25] Aranson I S *et al* 2005 *Phys. Rev. Lett.* **94** 037002
[26] Vestgarden J I, Shantsev D V, Galperin Y M and Johansen T H 2011 *Phys. Rev.* B **84** 1098–0121
[27] Vestgarden J I, Mikheenko P, Galperin Y M and Johansen T H 2013 *New J. Phys.* **15** 1367–2630
[28] Jing Z, Yong H D and Zhou Y H 2015 *Supercond. Sci. Technol.* **28** 075012
[29] Jing Z, Yong H D and Zhou Y H 2016 *Supercond. Sci. Technol.* **29** 105001
[30] Troyanovski A M, Aarts J and Kes P H 1999 *Nature* **399** 665
[31] Lee J, Wang H, Dreyer M, Berger H and Barker B I 2011 *Phys. Rev.* B **84** 060515
[32] Auslaender O M *et al* 2008 *Nat. Phys.* **5** 35
[33] Goa P E, Hauglin H, Baziljevich M, Il'yashenko E, Gammel P L and Johansen T H 2001 *Supercon. Sci. Technol.* **14** 729
[34] Kremen A, Wissberg S, Haham N, Persky E, Frenkel Y and Kalisky B 2016 *Nano Lett.* **16** 1626–30
[35] Raes B *et al* 2012 *Phys. Rev.* B **86** 064522
[36] Cole D, Bending S, Savel'ev S, Grigorenko A, Tamegai T and Nori F 2006 *Nat. Mater.* **5** 305
[37] Vasyukov D *et al* 2013 *Nat. Nanotechnol.* **8** 639
[38] Avraham N *et al* 2001 *Nature* **411** 451
[39] Cyrot M 1973 *Rep. Prog. Phys.* **36** 103
[40] Machida M and Kaburaki H 1993 *Phys. Rev. Lett.* **71** 3206–9
[41] Adami O A *et al* 2015 *Phys. Rev.* B **92** 134506
[42] He A, Xue C, Yong H D and Zhou Y H 2016 *Supercond. Sci. Technol.* **29** 065014
[43] Wai-Kwong K, Ulrich W, Andreas G, Alexei E K, Karen J K and George W C 2016 *Rep. Prog. Phys.* **79** 116501
[44] 'Shapiro I, Pechenik E and Shapiro B Y 2001 *Phys. Rev.* B **63** 184520
[45] Vodolazov D Y, Peeters F M, Morelle M and Moshchalkov V V 2005 *Phys. Rev.* B **71** 184502
[46] Machida M, Kano T, Koyama T, Kato M and Ishida T 2008 *J. Low Temp. Phys.* **151** 58–63
[47] Ota Y, Kobayashi K, Machida M, Koyama T and Nori F 2013 *IEEE Trans. Appl. Supercond.* **23** 2201105
[48] Berdiyorov G, Harrabi K, Oktasendra F, Gasmi K, Mansour A I, Maneval J P and Peeters F M 2014 *Phys. Rev.* B **90** 054506
[49] Jafri H M *et al* 2017 *J. Phys.: Condens. Matter* **29** 505701
[50] Embon L *et al* 2017 *Nat. Commun.* **8** 85
[51] Duarte E C S, Sardella E, Ortiz W A and Zadorosny R 2017 *J. Phys.: Condens. Matter* **29** 405605
[52] Kramer L and Watts-Tobin R J 1978 *Phys. Rev. Lett.* **40** 1041
[53] Watts-Tobin R J, Krähenbühl Y and Kramer L 1981 *J. Low Temp. Phys.* **42** 459
[54] Gladilin V N, Tempere J, Devreese J T, Gillijns W and Moshchalkov V V 2009 *Phys. Rev.* B **80** 054503
[55] Hernández A D and Domínguez D 2008 *Phys. Rev.* B **77** 224505
[56] Zhao H J, Misko V R, Peeters F M, Oboznov V, Dubonos S V and Grigorieva I V 2008 *Phys. Rev.* B **78** 104517
[57] Baruch-El E, Baziljevich M, Shapiro B Y, Johansen T H, Shaulov A and Yeshurun Y 2016 *Phys. Rev.* B **94** 054509
[58] Vestgården J I, Colauto F, de Andrade A M H, Oliveira A A M, Ortiz W A and Johansen T H 2015 *Phys. Rev.* B **92** 144510
[59] Brisbois J *et al* 2016 *Phys. Rev.* B **93** 054521